5 Water-Gas Shift Activity of Transition Metal SACs

In this chapter, we discuss our investigation on catalytic behaviour of transition metals (TMs) based SACs supported over AlN substrate (M@AlN; M=Ni, Pd, Pt, Cu, Ag, Au) towards water-gas shift (WGS) reaction, which is the reaction between CO and H_2O to produce CO_2 and H_2 molecule as a product. Here, we analysed the stability of M-atoms in terms of binding energy and diffusion of M-atom over substrate. The strong binding energy and high diffusion barrier confirms the stoned-stability of M@AlN and also restrict the cluster formation possibility of M@AlN. Further, by examinination of interaction of reactants with M@AlN confirms that the considered SACs are capable of handling individual/multiple reactants simultaneously. Further, we computed minimum energy path and studied complete reaction profile of the WGS reaction via formate and OH-assistive mechanisms over M@AlN and computed activation energy (E_a) using CI-NEB method. Overall, OH-assistive mechanism is found to be preferred over formate mechanism, with Au@AlN and Cu@AlN showing superior catalytic activity with E_a values 0.14 eV and 0.21 eV, respectively. The obtained E_a values are further validated with the linearity between E_a and co-adsorption energy of CO-OH molecule (E_{ads}(CO+OH)) and E_a and d-band center (ε_d), which is an accurate parameter to predict activity of TMs-based catalyst. Further the feasibility of the reaction is discussed in terms of relation between activation energy and reaction energy by employing energetic span model.

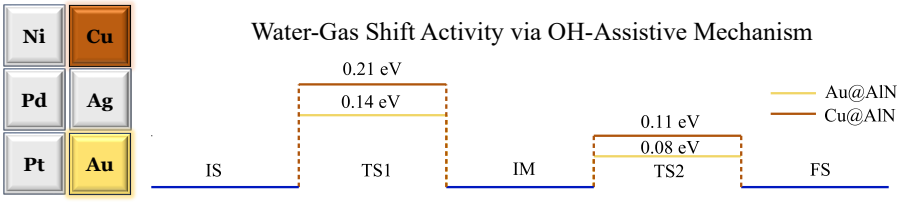

FIGURE 5.1: Graphical Abstract

5.1 Introduction

The global quest of renewable and sustainable energy sources and ozone-friendly industrial exercises has reinforced the chase for ingenious catalytic operations to produce green energy sources in heap[1]. Hydrogen gas (H_2) is been viewed as a shoo-in due to its ample abundancy, high energy value, compliance in usage and ecosystem and zero-carbon footprint. One of many ways to generate ultra-pure H_2 in plenty is water-gas shift (WGS) reaction, fundamentally a reversible reaction involving carbon monoxide (CO) and water vapour (H_2O) to produce carbon dioxide (CO_2) and H_2, represented as $CO + H_2O \rightleftarrows CO_2 + H_2$[2, 3]. The WGS reaction has reaped heightened emphasis from the research community and industries across globe due to its significance in production and purification of hydrogen, in syngas conditioning to maintain CO/H_2 ratio and its environmental impact as it converts detrimental CO gas into benign CO_2 gas, placing it amongst the prime chemical reactions[4]. Howbeit, the cardinal challenges in WGS reaction are (i) to manage its slow reaction kinetics and high thermodynamics of the reaction, (ii) to avert the CO poisoning effect of the catalyst, (iii) to oversee the selectivity of the catalyst towards forming H_2 as a product and not any other CH-products (like CH_3, CH_3OH etc.) and (iv) to implement large-scaled commercialization of such catalyst[5]. Thus, the WGS reaction, owing such an essentiality from environmental and industrial point of view, and having handful of complications, requires an auxiliary attention to study it's reaction kinetics and design an efficacious and potent catalyst for functional aspect.

Historically, TMs based catalysts like Ni(111), Ni(100), Ni(110), Ni(211)[6, 7] Pt-nanotubes[8], $Au_{32}M_6$ (M=Cu, Pt, Pd, Rh, Ir) nanoclusters (NCs)[9], Ag NCs[10] etc., are perceived to evince superior catalytic behaviour towards WGS reaction. However, their high cost, paucity and effectively low-metal-atom-utilization efficiency of the precious metals calls on us to look for an alternative approach to design a catalyst addressing the above issue at least without compromising the activity and selectivity for the WGS reaction. In that direction, an approach of retrenching the catalyst particle size from bulk to 2D to NCs and further to atomic scale is capturing interest, on the grounds of the fact that catalytic activity annexes eminently on downsizing the particle size[11, 12]. The amplified catalytic activity on reducing the size of the particle is due to the partially filled d-orbitals allowing it to possess variable oxidation states, also the introduction of

quantum confinement effect at an atomistic-scale leading to origination of frontier orbitals to interact with the reactants, leading to an optimum adsorption favourably assist the reaction[13, 14]. This lens of downsizing the particle size led to an entirely new domain in heterogeneous catalysis, now known as single-atom catalysts (SACs), wherein an atomically dispersed/implanted/embedded atoms moored by some porous substrates, serves as an active centre for the reaction, has procured keen attention of the researchers in past decade or so[15–17]. In the recent years, many SACs has been probed by both theoretical as well as experimental angle for WGS reaction like TM/ZnO (TM: Mn, Fe, Co, Ni)[18] Cu/α-MoC[19], Ir_1/FeO_x[20], Ir_1/α-MoC(111)[21], M_1/α-MoC(100) (M=Rh, Pd, Pt, Au)[22], Pt/TiO_2[23, 24], Ru/FeO_x[25] etc.. Although, various combination of SACs and substrates are scouted and scanned in this regard, but majority of the work is performed over carbon-based or oxide surfaces owing to their abundancy, stability and high-porosity[26, 27]. Moreover, the lattice oxygen of oxide surface also assists in the redox mechanism of WGS reaction. Having said that, the key challenges for oxide surfaces is managing its complex surface chemistry, maintaining reaction specificity and achieving commercial scalability. As the substrate plays an instrumental role, not only in anchoring and stabilizing dispersed atoms, but it also reshapes its electronic structure, promoting catalytical activity and productivity of SACs[28]. So, a comprehensive study on the catalytical property of SACs supported over a substrate for WGS reaction would prove to be a great deal to design a practical catalyst.

Thus, here, we contemplated AlN substrate to anchor TM SACs, hereafter noted as M@AlN (M=Ni, Pt, Pd, Cu, Ag, Au), and inspected its structure-electronic features, interaction mechanistic of reactants and then the electrocatalytic behaviour towards WGS reaction via two reaction mechanisms; (i) formate mechanism[29] and (ii) OH-assistive mechanism[22]. The complete reaction profiles of these mechanism are discussed later in the article. The rationale behind choosing AlN as a substrate is its excellent thermal conductivity and terrific thermal as well as chemical stability makes it efficiently operational under extreme reaction condition and can tackle high thermodynamics of WGS reaction[30, 31]. This research paper manifest a thorough analysis of fundamental principles governing the WGS reaction and its critical role in the evolving landscape of clean energy production and industrial sustainability, also foretell a future possibility for designing a rational, potent and economically practicable SACs.

5.2 Methodology

5.2.1 Total Energy Calculation

We used Quantum ESPRESSO simulation package based on density functional theory (DFT) to perform all the self-consistent total energy calculations[32, 33]. All the calculations were done considering spin-polarization as the considered systems involve TMs. To consider electron-ion interactions, we considered all-electron projected augmented wave (PAW) pseudo-potentials[34, 35]. To evaluate electronic exchange-correlation interactions, generalized gradient approximation (GGA) in the framework of Perdew–Burke–Ernzerhof (PBE) were used[36]. , The semi-empirical van der Waals corrections DFT-D3 proposed by Grimme et. al were employed to consider the long-range dispersion forces[37]. A vacuum of 18 Å was provided in **z**-direction to avoid interaction between two periodic images. The kinetic energy cut-off of 80 Ry was chosen to be for the plane-wave basis set. For geometry optimization, the convergence threshold set to 1.0×10^{-6} eV without applying any symmetry constraints. The Marzari-Vanderbilt smearing method with a finite temperature width of 0.02 Ry was adopted[38]. Supercells consisting of $4 \times 4 \times 1$ AlN unit cell were used and the Brillouin zones were sampled using a Monkhorst–Pack scheme with $8 \times 8 \times 1$ **k**-points grid[39].

5.2.2 Minimum Energy Path and Activation Energy Computation

The reaction profiles of WGS reaction were examined using the climbing image nudged elastic band (CI-NEB) method. (implemented in the Quantum ESPRESSO) [40, 41]. The activation energy barrier (E_a) for each reaction step was obtained using the following formula

$$E_a = E_{TS} - E_{IS/IM} ...(4)$$

Where E_{TS} and $E_{IS/IM}$ are the energies of transition state, initial/intermediate state (depend on the nature of reaction). In our study, XCrySDen visualization package was used to prepare all visual depictions of the structures under investigation[42].

5.3 Results and Discussion

5.3.1 Structural Analysis

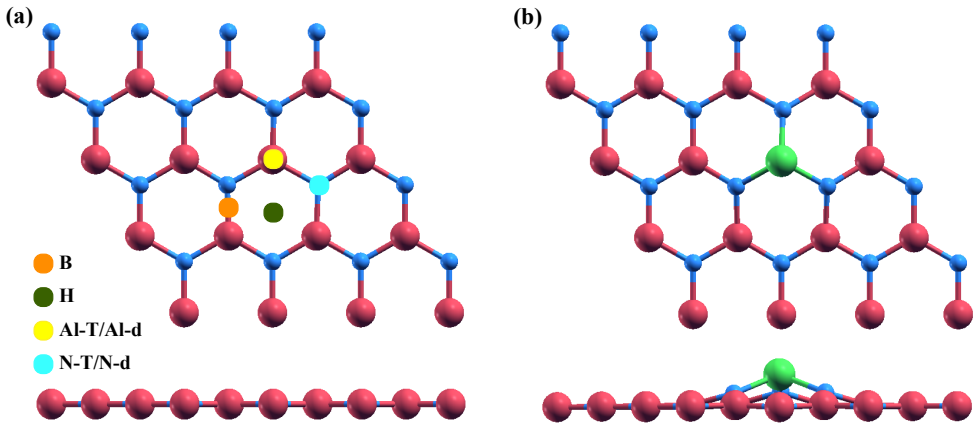

FIGURE 5.2: Top and side view of (a) optimized geometry of AlN supercell with representation of possible anchoring sites for SACs and (b) Top and side view of M@AlN (M=Ni, Pd, Pt, Cu, Ag, Au) at the Al-d site. Red, light blue and light green sphere represents Al, N and M-atom, respectively.

As stated in introduction part, we considered M@AlN (M=Ni, Pd, Pt, Cu, Ag, Au) SACs to study WGS reaction activity. Before going for the reactant adsorption and reaction kinetics, it is crucial to investigate structural stability of these SACs. In our study, we considered 4 x 4 supercell of AlN to anchor the SACs. As shown in the Fig5.2(a) an AlN sheet forms a graphene like structure, having various possible anchoring site to disperse a SAC viz., Al-top (Al-T), N-top(N-T), bridge(B), hollow(H), Al-defect(Al-d) and N-defect(N-d). In our calculation, we examined all these sites for each SACs and calculated binding energy of M over these sites is calculated as $E_b(M) = E_{M@AlN} - E_{AlN} - E_M$ and is mentioned in table1 (in SI). It can be observed from the table that Al-d site as pictured in Fig5.2(b) is found to be most stable for all considered SACs with binding energy <-4.00 eV , evincing a strong interaction between embedded atom and substrate, a prerequisite condition for a stable SACs. So, further calculations were carried out using M@AlN at Al-d site. To further look into stability of M@AlN, we computed diffusion of metal atoms from the Al-d site to neighbouring Al-d site by means of CI-NEB method. A complete diffusion pathway and corresponding diffusion barrier for considered SACs is displayed in. As shown in Fig5.3, the computed diffusion barrier for M@AlN is greater than 4.00 eV, showing it is difficult for SACs to diffuse over the substrate, highlighting the immobility of the dispersed atoms,

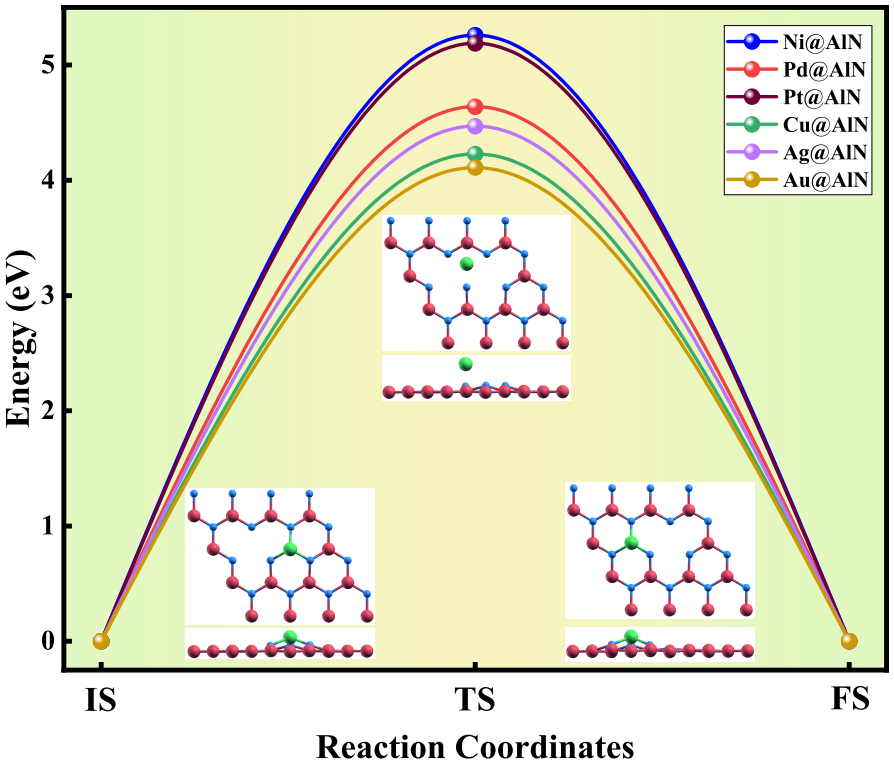

FIGURE 5.3: The diffusion pathway and corresponding energy profile of M-atom from one Al-d site to nearest Al-d site. The corresponding geometries for initial state (IS), transition state (TS) and final state (FS) are represented inset.

abandoning the cluster formation possibility of SACs, which is an indispensable precondition to design a stoned-stable and perdurable SACs.

5.3.2 Interaction of Reactants with M@AlN and Reaction Mechanisms

In order to understand any reaction kinetics, it is of great significance to study and analyse the insights of reactant interaction with the catalyst. As specified above, we considered two reaction mechanisms of WGS reaction namely, formate and OH assistive mechanism, thus, here we have discussed both the mechanisms and interaction of reactants corresponding to particular mechanism. The optimized geometries of adsorbed/co-adsorbed reactants (CO, OH, H_2O, CO+OH, CO+H_2O) are depicted in Fig5.4. The adsorption/co-adsorption energies of reactants (CO, OH, H_2O, CO+OH, CO+H_2O) and the binding energy of M@AlN are graphed in Fig5.5.

$$E_{ads} = E_{molecule+M@AlN} - E_{M@AlN} - E_{molecule}$$

where, $E_{molecule+M@AlN}$, $E_{M@AlN}$ and $E_{molecule}$ are the total energy of single/co-adsorbed molecule over M@AlN, energy of M@AlN and energy of isolated molecule.

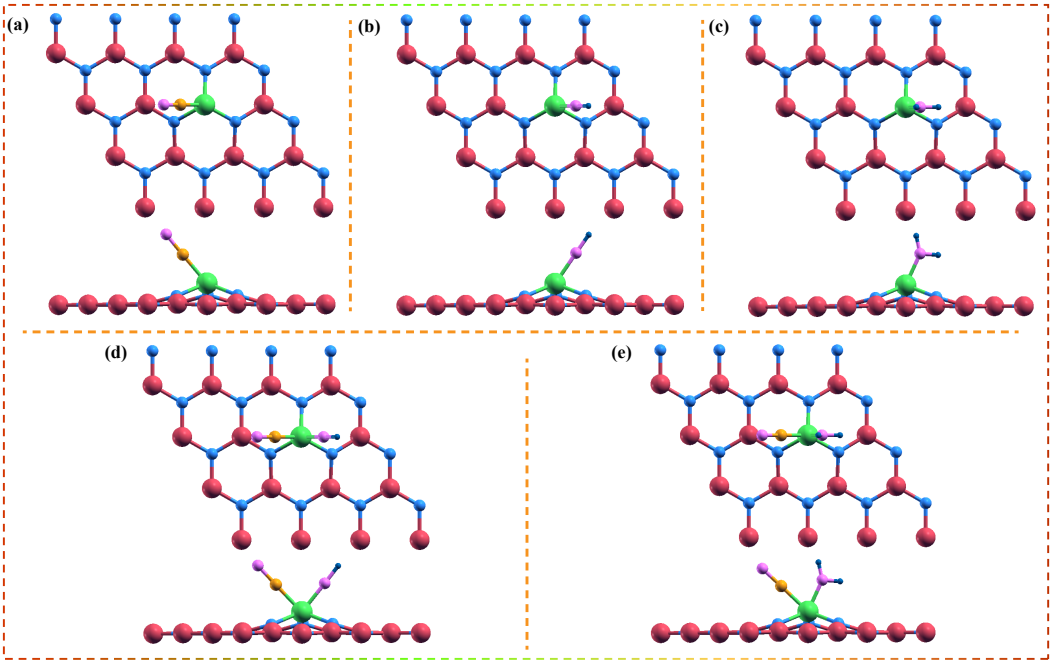

FIGURE 5.4: Optimized geometry of (a) CO, (b) OH, (c) H_2O, (d) CO+OH and (e) CO+H_2O adsorbed M@AlN. Orange, purple and blue sphere represent C, O and H-atom, respectively.

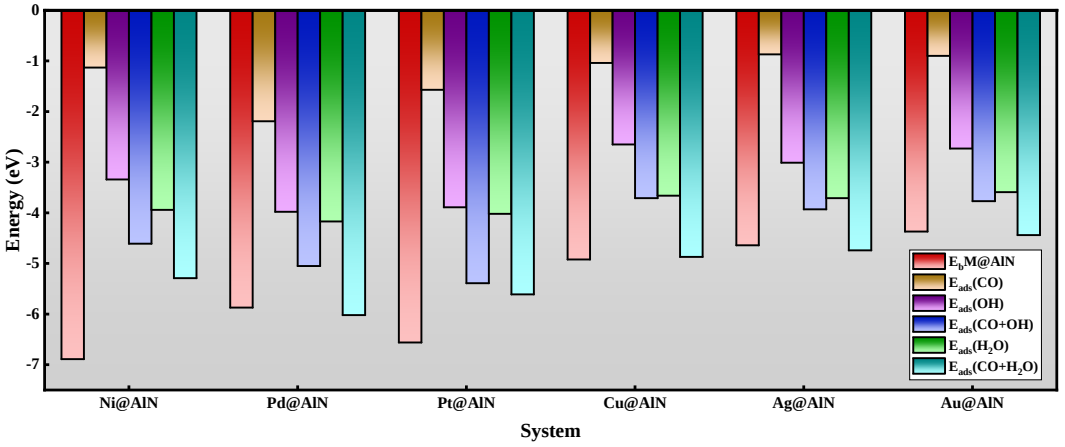

FIGURE 5.5: A plot of binding energy (E_b) of M@AlN and adsorption/co-adsorption (E_{ads}) energies of reactants over M@AlN.

5.3.2.1 Formate Mechanism

The formate mechanism of WGS reaction was first explored by Campbell and Daube on a single crystal copper catalyst. In this mechanism, the initial state comprises of co-adsorbed CO and H_2O molecule, thereafter the H2O molecule dissociate (H^+-OH^-) to form a surface hydroxyl (R-OH), which then combine with the CO molecule to form a formate complex. The formate complex then leaves H^+ to react with H^+ (earlier dissociated from H_2O) to form H_2 and CO_2 as a product. As it can be observed from table 1 (in SI), the adsorption energy of CO molecule -0.87 eV to -2.19 eV for the considered systems and H_2O adsorption energy ranges -3.59 eV to -4.17 eV, suggesting that the interaction of H_2O is more prominent than that of CO, which means that the CO contamination effect over M@AlN would also likely to be curtailed, indeed impacting longevity of the SACs. Further, from the co-adsorption energy of CO + H_2O, it can be concluded that concurrent interaction of reactants is too stronger than individual ones, fostering the condition to initiate the reaction favourably.

5.3.2.2 OH-Assistive Mechanism

The fairly new and little studied mechanism is OH-assistive mechanism, in which instead of H_2O, the reaction initiates with OH and CO molecule concurrently adsorbed over active site, reacting to form carboxyl-type (O*COH) complex, which would then react with another OH molecule, to dissociate into CO_2 and H_2O (rather than H_2) as a product. As it can be observed from the table 1 (in SI), the interaction energy of OH (ranges from -2.65 eV to -3.98 eV) is relatively higher than that of CO, shows the considered SACs have stronger affinity towards OH molecule than CO, abetting in lowering catalyst deactivation by CO sorption. Moreover, the co-adsorption energy of CO+OH (-3.68 eV to -5.39 eV) molecules is much higher than that of individual molecules, indicating that the considered SACs are competent of operating poly-adsorbates in unison.

5.3.3 Minimum Energy Path and Activation Energy Calculations

5.3.3.1 Formate Mechanism

First, we considered traditional and familiar formate mechanism to investigate WGSR activity of M@AlN. As discussed above, the reaction begins with co-adsorbed CO and H_2O molecule, subsequently, the H_2O molecule break into H^+-OH^- (TS1) to form hydroxyl complex (M-OH), which further settles in as separately adsorbed H^* and OH^* intermediates, the formation of these intermediates is found to be the RDS of the reaction. Further, the hydroxyl complex reacts

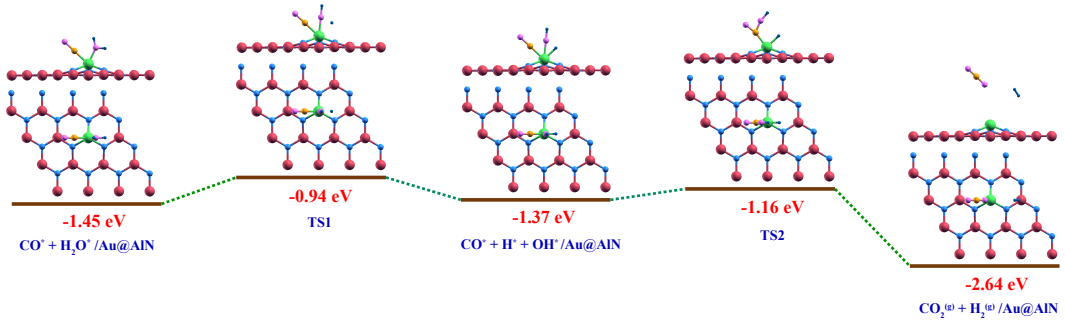

FIGURE 5.6: The complete reaction profile and optimized geometric configurations of various states for WGS reaction via formate mechanism on Au@AlN.

with CO to form a formate, which then dissociate into $CO_2^{(g)}$ and $H_2^{(g)}$. The complete reaction profile over Au@AlN is depicted in Fig5.6, and the reaction profiles over other M@AlN (M=Ni, Pd, Pt, Cu, Ag), is presented in SI (Fig.1 to Fig.5). Moreover, the complete energy profile of the reaction over M@AlN is presented schematically in Fig5.7(a). The activation energies and reaction energies for all the systems are tabulated in table 2 (in SI). As the values suggests, the activation energy for Au@AlN is found to be lowest i.e., 0.51 eV and 0.21 eV for first and second barrier respectively, whereas these values range in 0.68 eV to 1.16 eV for first barrier and 0.29 eV to 0.45 eV for second barrier for other considered SACs. Although, Au@AlN shows reasonably good activity towards WGS reaction via formate mechanism, but to further corroborate the activity and have an in-depth insight, we considered another mechanism of WGS reaction.

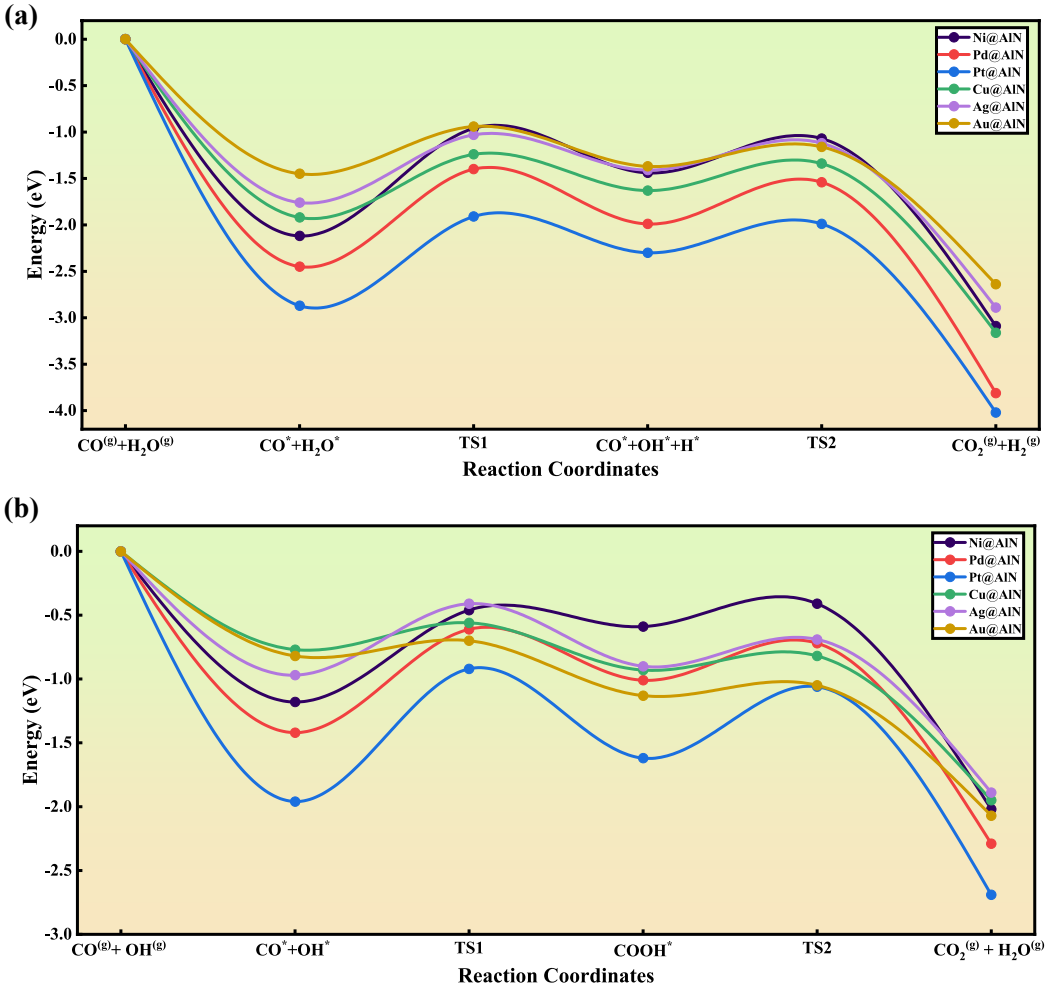

FIGURE 5.7: The complete energy profile for WGS reaction via (a) formate mechanism and (b) via OH-assistive mechanism over M@AlN.

5.3.3.2 OH-Assistive Mechanism

A kind of new and little explored OH-assistive mechanism was considered, wherein the reaction mechanism as discussed above, begins with co-adsorbed CO-OH molecule, reacting to form a COOH-complex, further it reacts with OH-molecule to dissociate into $CO_2^{(g)}$ and H_2O. In this reaction, the formation of COOH-complex is found to be the RDS of the reaction. The complete reaction profile over Au@AlN is pictured in Fig5.8, and the reaction profiles over other M@AlN (M=Ni, Pd, Pt, Cu, Ag), is presented in SI (Fig.6 to Fig. 9). Moreover, the complete energy profile of the reaction over M@AlN is sketched in Fig5.7(b). The activation energies and reaction energies for all the systems are indexed in table 3 (in SI). As the values suggests, the activation energy for Au@AlN is turned out to be exceptionally low viz., 0.14 eV and 0.08 eV for first and second barrier respectively. In conjunction

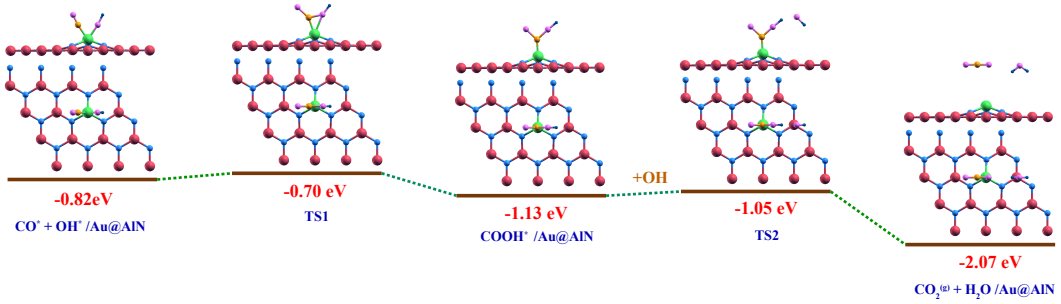

FIGURE 5.8: The complete reaction profile and optimized geometric configurations of various states for WGS reaction via OH-assistive mechanism on Au@AlN.

with Au@AlN, Cu@AlN as well shows fairly good catalytic activity with energy barriers (0.21 eV and 0.11 eV) slightly higher than Au@AlN as shown in Fig5.9, indicating the workability of the mechanism over relatively economical Cu-SACs too. The energy barriers for other considered M@AlN (M=Ni, Pd, Pt, Ag) ranges in 0.56 eV to 1.04 eV for first barrier and 0.18 eV to 0.56 eV for second barrier, respectively.

From the above discussion, inference could be drawn that, overall, the OH-assistive mechanism of WGS reaction is more probable as compared to formate mechanism and Au@AlN and Cu@AlN could potentially be a worthy candidate for all-important WGS reaction, preferring OH-assistive mechanism of the reaction.

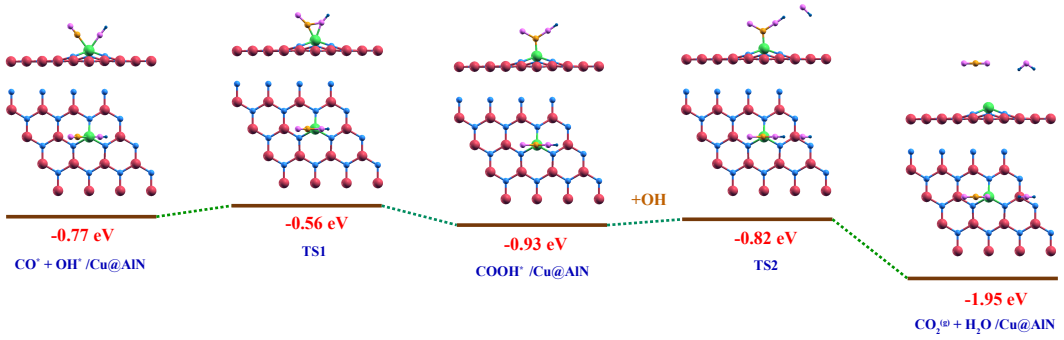

FIGURE 5.9: The complete reaction profile and optimized geometric configurations of various states for WGS reaction via OH-assistive mechanism on Cu@AlN.

5.4 Validating the CI-NEB Results

The adsorption/co-adsorption strength of the reactants with the catalyst is a crucial parameter affecting the overall performance of the catalyst. According to

the Sabatier principle, the interaction of reactants with the catalyst should be optimum in order to design an efficiently practical catalyst as if the interaction of reactants is too weak, the catalyst will not be able hold the reactants during the breaking and making of bonds process, and if the interaction is too strong, the catalyst will not be able to release the products formed after the reaction efficiently. So, the overall reaction performance of a catalyst is greatly influenced by the how the catalyst interacts with the catalyst. So, to analyse and validate the activation energy results of the WGS reaction via OH-assistive mechanism over M@AlN, we plot a relationship between the activation energy of the RDS, i.e., formation of COOH complex from the co-adsorbed CO-OH molecules and the co-adsorption energy of CO+OH molecule as presented in Fig5.10(a). The fairly linear relationship between activation energy and co-adsorption energy of CO-OH molecule, thus validate the performance of M@AlN SACs.

Although, the interaction energy is a good parameter to judge the performance

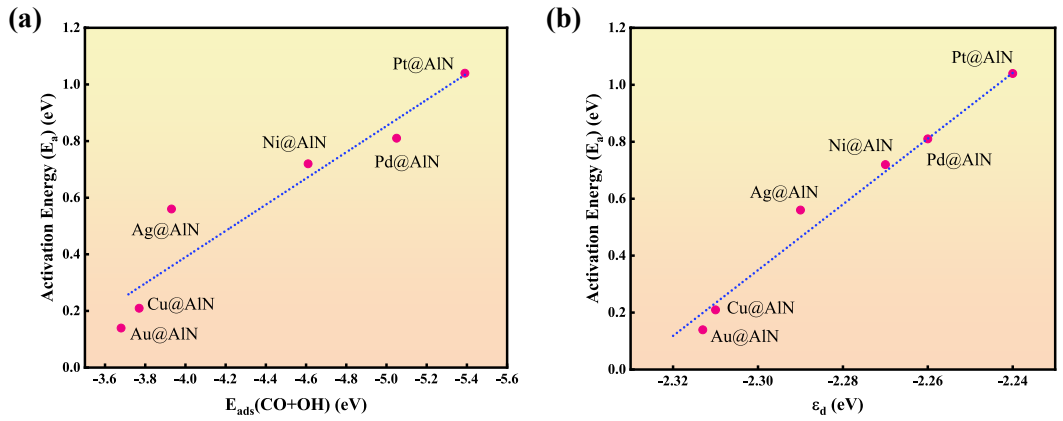

FIGURE 5.10: Relationship between (a) activation energy (E_a) and co-adsorption energy of CO-OH molecule on M@AlN and (b) activation energy (E_a) and ε_d, for M@AlN.

of the catalyst, but first B. Hammer and J. K. Norskov and later S. Bhattacharjee at al., designed and developed a model viz., for predicting the chemical activity of TM-based catalyst by analyzing the electronic properties of the catalyst via an electronic reactivity descriptor like d-band center(ε_d), by analyzing projected density of states of d-orbitals of TM and is calculated as

$$\varepsilon_d = \frac{\int_{-\infty}^{E_F}(E-E_F)D_{d\sigma}(E)dE}{\int_{-\infty}^{E_F}D_{d\sigma}(E)dE} \ .$$

Where $D_{d\sigma}(E)dE$ ($\sigma = \uparrow, \downarrow$) is the DOS projected on the d-states of Co atom, E is the energy and E_F is the Fermi energy of the system[43–45].

The ε_d represents an average energy of d-band and it retorts the interaction between reactants and TM-based catalyst. The ε_d values suggests that the farther(closer) the ε_d from the fermi level, there are a smaller(larger) number of empty anti-bonding states of TM available to take part in interaction, resulting in weaker(stronger) interaction with the reactants, thereby suggesting faster(slower) reaction possibility[46]. Thus, we plot the relationship between activation energy and ε_d values as shown in Fig5.10(b), and remarkably good linear nature exhibited by the plot, with lowest value of ε_d for Au@AlN in fine agreement with lowest value of activation energy for the same, and also the trend remaining consistent, authenticate our results of activity of M@AlN for WGS reaction.

5.5 Feasibility of the Reaction

In any catalytic reaction, along with the activation energy (E_a), the reaction energy (E_R), which is the energy difference between initial and final state, is also a critical parameter to gauge the catalyst performance, as it gives an indication about the thermicity of the reaction like if the energy of initial state is higher(lower) than the energy of final state, the reaction would be exothermic(endothermic). A common energy profile of an exothermic reaction is presented in Fig5.11(a), to pictorially show the two parameters. According to the energetic span model (ESM)[47, 48], the catalytic cycle, which started from IS, require some activation energy E_a, and the cycle ends on FS, releasing E_R amount of energy. Hereon, considering the cyclic nature of reaction, the second cycle of the reaction would start from the energy level of FS and not from the energy level of IS. This deliberation ensures that the energy released (E_R) in the first cycle, can subsequently be utilized in the second cycle to compensate the activation energy demand, and the reaction persists without needing any external energy then. Employing this concept in our study, as plotted in Fig5.11(b), the values of E_a (blue sphere) and E_R (red sphere) for considered M@AlN for OH-assistive mechanism of WGS reaction, it is noticeable that for Ni/Pd/Pt@AlN, the value of E_R is either less or nearly equal to the E_a, cramping the possibility of sustained reaction for multiple cycles. Whereas, in the case of Cu/Ag/Au@AlN, the E_R value is significantly higher than that of E_a (especially for Au/Cu@AlN), propping the usability of Au@AlN and Cu@AlN for prolonged period of time for an efficient and feasible WGS reaction via OH-assistive mechanism.

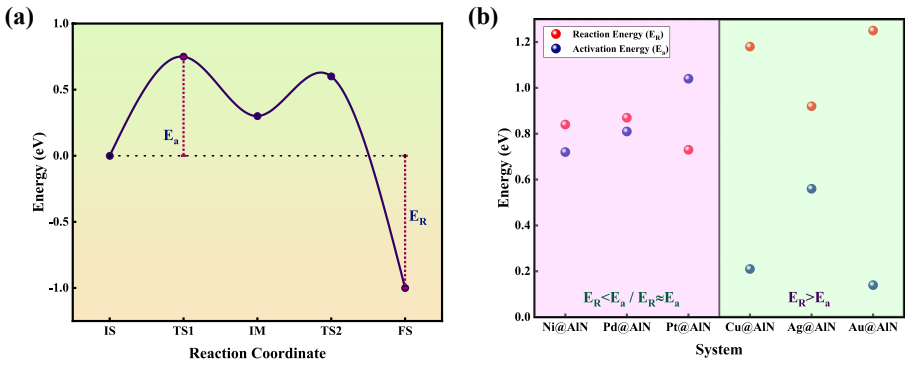

FIGURE 5.11: (a) A general energy profile for an exothermic reaction and (b) a comparision between activation energy (E_a) and reaction energy (E_R) of WGS reaction via OH-assistive mechanism on M@AlN.

5.6 Conclusion

Our study shed a light on potentiality of TM SACs, viz., M@AlN (M=Ni, Pd, Pt, Cu, Ag, Au), towards the WGS reaction by means of DFT calculations. To anchor the considered SACs, a 2D sheet of AlN is employed, and all possible anchoring sites are considered, with Al-d site emerging out as preferable site for M-atom embedding with significantly higher binding energy. The substantially higher diffusion barrier insinuates at the stoned-stability of M@AlN, obviate the cluster-aggregation probability, thus improving the persevering applicability. Afterwards, the assessment of interaction of reactants with M@AlN conveyed that the considered SACs are adroit in capturing individual/multiple reactants concurrently. To examine the WGS reaction activity of M@AlN, the formate mechanism and OH-assistive mechanism was considered. As a whole, the OH-assistive mechanism over M@AlN became apparent as compared to the formate mechanism. Concretely, the Au@AlN and Cu@AlN are recognized as optimal and peerless candidates towards WGS reaction preferring OH-assistive mechanism, with the activation energy of RDS is as low as 0.14 eV and 0.21 eV, respectively. The linear nature between E_a and E_{ads}(CO+OH) and E_a and ε_d authenticate our reaction mechanism findings. Moreover, according to energetic span model, the comparison between E_a and reaction energy (E_R) ascertains the feasibility and expediency of Au@AlN and Cu@AlN towards WGS reaction. Ergo, our research provides an extensive computational path of scheming an efficient and practicable SACs for WGS reaction.

Bibliography

[1] Y. Chen, J. Lin and X. Wang. *Chemical Communications*, 58(2):208–222, 2022.

[2] P. Ebrahimi, A. Kumar and M. Khraisheh. *Emergent Materials*, 3:881–917, 2020.

[3] C. Ratnasamy and J. P. Wagner. *Catalysis Reviews*, 51(3):325–440, 2009.

[4] W.-H. Chen and C.-Y. Chen. *Applied Energy*, 258:114078, 2020.

[5] L. Zhou, Y. Liu, S. Liu *et al. Journal of Energy Chemistry*, 2023.

[6] R. C. Catapan, A. A. Oliveira, Y. Chen *et al. The Journal of Physical Chemistry C*, 116(38):20281–20291, 2012.

[7] A. Mohsenzadeh, T. Richards and K. Bolton. *Surface Science*, 644:53–63, 2016.

[8] J. L. Fajin and M. N. D. Cordeiro. *Applied Catalysis B: Environmental*, 263:118301, 2020.

[9] L. Fang, T. Chen, Y. Meng *et al. Molecular Catalysis*, 483:110757, 2020.

[10] A. Arab, D. Sharafie and M. Fazli. *Journal of Physics and Chemistry of Solids*, 109:100–108, 2017.

[11] L. Liu and A. Corma. *Chemical reviews*, 118(10):4981–5079, 2018.

[12] Z. Chen, L. Chen, C. Yang *et al. Journal of Materials Chemistry A*, 7(8):3492–3515, 2019.

[13] A. Wang, J. Li and T. Zhang. *Nature Reviews Chemistry*, 2(6):65–81, 2018.

[14] Z. Fu, B. Yang and R. Wu. *Physical review letters*, 125(15):156001, 2020.

[15] B. Qiao, A. Wang, X. Yang *et al. Nature chemistry*, 3(8):634–641, 2011.

[16] S. Mitchell and J. Pérez-Ramírez. *Nature communications*, 11(1):1–3, 2020.

[17] S. K. Kaiser, Z. Chen, D. Faust Akl *et al. Chemical reviews*, 120(21):11703–11809, 2020.

[18] X.-K. Gu, C.-Q. Huang and W.-X. Li. *Catalysis Science & Technology*, 7(19):4534–4534, 2017.

[19] X.-Y. Zou, L. Mi, Z.-J. Zuo *et al. Journal of Molecular Modeling*, 26:1–7, 2020.

[20] J.-X. Liang, J. Lin, J. Liu *et al. Angewandte Chemie*, 132(31):12968–12975, 2020.

[21] L. Sun, J. Xu, X. Liu *et al. ACS Catalysis*, 11(10):5942–5950, 2021.

[22] J. Li, L. Sun, Q. Wan *et al. The Journal of Physical Chemistry Letters*, 12(46):11415–11421, 2021.

[23] S. C. Ammal and A. Heyden. *ACS Catalysis*, 7(1):301–309, 2017.

[24] S. C. Ammal and A. Heyden. *Chemie Ingenieur Technik*, 89(10):1343–1349, 2017.

[25] J. Guan, J. Liu, Y. Jin *et al.*

[26] M. B. Gawande, P. Fornasiero and R. Zboril. *Acs Catalysis*, 10(3):2231–2259, 2020.

[27] H. Fei, J. Dong, D. Chen *et al. Chemical Society Reviews*, 48(20):5207–5241, 2019.

[28] S. Tauster, S. Fung and R. L. Garten. *Journal of the American Chemical Society*, 100(1):170–175, 1978.

[29] E. Baraj, K. Ciahotnỳ and T. Hlinčík. *Fuel*, 288:119817, 2021.

[30] K. Miwa and A. Fukumoto. *Physical Review B*, 48(11):7897, 1993.

[31] J. Ben, X. Liu, C. Wang *et al. Advanced Materials*, 33(27):2006761, 2021.

[32] P. Giannozzi, S. Baroni, N. Bonini *et al. Journal of physics: Condensed matter*, 21(39):395502, 2009.

[33] P. Giannozzi, O. Andreussi, T. Brumme *et al. Journal of physics: Condensed matter*, 29(46):465901, 2017.

[34] P. E. Blöchl. *Physical review B*, 50(24):17953, 1994.

[35] G. Kresse and D. Joubert. *Physical review b*, 59(3):1758, 1999.

[36] J. P. Perdew, K. Burke and M. Ernzerhof. *Physical review letters*, 77(18):3865, 1996.

[37] S. Grimme, J. Antony, S. Ehrlich *et al. The Journal of chemical physics*, 132(15):154104, 2010.

[38] N. Marzari, D. Vanderbilt, A. De Vita *et al. Physical review letters*, 82(16):3296, 1999.

[39] H. J. Monkhorst and J. D. Pack. *Physical review B*, 13(12):5188, 1976.

[40] G. Henkelman and H. Jónsson. *The Journal of chemical physics*, 113(22):9978–9985, 2000.

[41] G. Henkelman, B. P. Uberuaga and H. Jónsson. *The Journal of chemical physics*, 113(22):9901–9904, 2000.

[42] A. Kokalj. *Journal of Molecular Graphics and Modelling*, 17(3-4):176–179, 1999.

[43] B. Hammer and J. K. Nørskov. In *Advances in catalysis*, volume 45, pages 71–129. Elsevier, 2000.

[44] S. Bhattacharjee, U. V. Waghmare and S.-C. Lee. *Scientific reports*, 6(1):1–10, 2016.

[45] B. A. Baraiya, H. Tanna, V. Mankad *et al. The Journal of Physical Chemistry A*, 125(24):5256–5272, 2021.

[46] H. Xin, A. Vojvodic, J. Voss *et al. Physical Review B*, 89(11):115114, 2014.

[47] S. Kozuch and S. Shaik. *Accounts of chemical research*, 44(2):101–110, 2011.

[48] S. Kozuch. *Wiley Interdisciplinary Reviews: Computational Molecular Science*, 2(5):795–815, 2012.